# Detailed Study of Four-wave Mixing in Raman DFB Fiber Lasers

**Jindan Shi[1,2],[*] Peter Horak[1], Shaif-ul Alam[1] and Morten Ibsen[1]**

[1]*Optoelectronics Research Centre, University of Southampton, SO17 1BJ, UK*
[2]*State Key Laboratory of Information Photonics and Optical Communication, Beijing University of Posts and Telecommunications, Beijing 100876, China*
[*]*sjdbupt@gmail.com*

**Abstract:** We both experimentally and numerically studied the ultra-compact wavelength conversion by using the four-wave mixing (FWM) process in Raman distributed-feedback (R-DFB) fiber lasers. The R-DFB fiber laser is formed in a 30 cm-long commercially available Ge/Si standard optical fiber. The internal generated R-DFB signal acts as the pump wave for the FWM process and is in the normal dispersion range of the fiber. Utilizing a tunable laser source as a probe wave, FWM frequency conversion up to ~40 THz has been demonstrated with conversion efficiency > -40 dB. The principle of such a wide bandwidth and high conversion efficiency in such a short R-DFB cavity has been theoretically analyzed. The simulation results match well with the experimental data.



**OCIS codes:** (060.3735) Fiber Bragg gratings; (190.4380) Nonlinear optics, four-wave mixing; (060.3510) Lasers, fiber.

## References and links

1. Z. Jianhui, P. Namkyoo, K. J. Vahala, M. A. Newkirk, and B. I. Miller, "Four-wave mixing wavelength conversion efficiency in semiconductor traveling-wave amplifiers measured to 65 nm of wavelength shift," IEEE Photon. Technol. Lett. **6**, 984-987 (1994).
2. F. Girardin, J. Eckner, G. Guekos, R. Dall'Ara, A. Mecozzi, A. D'Ottavi, F. Martelli, S. Scotti, and P. Spano, "Low-noise and very high-efficiency four-wave mixing in 1.5-mm-long semiconductor optical amplifiers," IEEE Photon. Technol. Lett. **9**, 746-748 (1997).
3. H. Kuwatsuka, H. Shoji, M. Matsuda, and H. Ishikawa, "Nondegenerate four-wave mixing in a long-cavity λ/4-shifted DFB laser using its lasing beam as pump beams," IEEE J. Quantum Electron. **33**, 2002-2010 (1997).
4. H. Kuwatsuka, H. Shoji, M. Matsuda, and H. Ishikawa, "THz frequency conversion using nondegenerate four-wave mixing process in a lasing long-cavity λ/4-shifted DFB laser," Electron. Lett. **31**, 2108-2110 (1995).
5. B. E. Little, H. Kuwatsuka, and H. Ishikawa, "Nondegenerate four-wave mixing efficiencies in DFB laser wavelength converters," IEEE Photon. Technol. Lett. **10**, 519-521 (1998).
6. H. Fukuda, K. Yamada, T. Shoji, M. Takahashi, T. Tsuchizawa, T. Watanabe, J.-i. Takahashi, and S.-i. Itabashi, "Four-wave mixing in silicon wire waveguides," Opt. Express **13**, 4629-4637 (2005).
7. H. Hu, C. Peucheret, M. Pu, H. Ji, M. Galili, K. Yvind, J. M. Hvam, P. Jeppesen, and L. K. Oxenløwe, "Wavelength Conversion with Large Signal-Idler Separation using Discrete Four-Wave Mixing in a Silicon Nanowire," in *CLEO: Science and Innovations (CLEO: S and I)*, OSA Technical Digest (online) (Optical Society of America, 2012), CW1A.2.
8. K. Inoue and H. Toba, "Wavelength conversion experiment using fiber four-wave mixing," IEEE Photon. Technol. Lett. **4**, 69-72 (1992).
9. O. Aso, A. Shin-Ichi, T. Yagi, M. Tadakuma, Y. Suzuki, and S. Namiki, "Broadband four-wave mixing generation in short optical fibres," Electron. Lett. **36**, 709-711 (2000).
10. K. Inoue, "Four-wave mixing in an optical fiber in the zero-dispersion wavelength region," J. Lightwave Technol. **10**, 1553-1561 (1992).
11. K. Inoue, "Arrangement of fiber pieces for a wide wavelength conversion range by fiber four-wave mixing," Opt. Lett. **19**, 1189-1191 (1994).
12. A. Zhang and M. S. Demokan, "Broadband wavelength converter based on four-wave mixing in a highly nonlinear photonic crystal fiber," Opt. Lett. **30**, 2375-2377 (2005).

13. X. Feng, F. Poletti, A. Camerlingo, F. Parmigiani, P. Petropoulos, P. Horak, G. M. Ponzo, M. Petrovich, J. Shi, W. H. Loh, and D. J. Richardson, "Dispersion controlled highly nonlinear fibers for all-optical processing at telecoms wavelengths," Opt. Fiber Technol. **16**, 378-391 (2010).
14. D. Méchin, R. Provo, J. D. Harvey, and C. J. McKinstrie, "180-nm wavelength conversion based on Bragg scattering in an optical fiber," Opt. Express **14**, 8995-8999 (2006).
15. J. Shi, S.-u. Alam, and M. Ibsen, "Ultrawide-range four-wave mixing in Raman distributed-feedback fiber lasers," Opt. Lett. **38**, 944-946 (2013).
16. J. Shi, S.-U. Alam, and M. Ibsen. "Ultra-Broadband Wavelength Conversion Based on Four-Wave Mixing in a Raman DFB Fiber Laser, " in *Optical Fiber Communication Conference/National Fiber Optic Engineers Conference 2013*, OSA Technical Digest (online) (Optical Society of America, 2013), paper JW2A.23.
17. J. Shi, S.-U. Alam, and M. Ibsen, "Sub-watt threshold, kilohertz-linewidth Raman distributed-feedback fiber laser," Opt. Lett. **37**, 1544-1546 (2012).
18. J. Shi, S.-U. Alam, and M. Ibsen, "Highly efficient Raman distributed feedback fibre lasers," Opt. Express **20**, 5082-5091 (2012).
19. M. Ibsen, M. K. Durkin, M. J. Cole, and R. I. Laming, "Sinc-sampled fibre Bragg gratings for identical multiple wavelength operation," IEEE Photon. Technol. Lett. **10**, 842-844 (1998).
20. G. Agrawal, *Nonlinear Fiber Optics,* Third ed. (Springer Berlin / Heidelberg, 2000).
21. W. H. Loh, B. N. Samson, and J. P. d. Sandro, "Intensity profile in a distributed feedback fiber laser characterized by a green fluorescence scanning technique," Appl. Phys. Lett. **69**, 3773-3775 (1996).
22. I. V. Kabakova, T. Walsh, C. M. de Sterke, and B. J. Eggleton, "Performance of field-enhanced optical switching in fiber Bragg gratings," J. Opt. Soc. Am B **27**, 1343-1351 (2010).
23. Y. Hu and N. G. R. Broderick, "Improved design of a DFB Raman fibre laser," Opt. Commun. **282**, 3356-3359 (2009).
24. Q. Zeng, "Dispersive properties in phase-shifted Bragg grating filters," in *Antennas and Propagation Society International Symposium, 1998. IEEE*, 1998), 1060-1063 vol.1062.

## 1. Introduction

Wavelength conversion based on the FWM technique has attracted significant attention in the area of nonlinear optics for more than two decades. FWM has been realized in several nonlinear media, such as semiconductor travelling-wave amplifier (TWA) [1], semiconductor optical amplifiers (SOA) [2], semiconductor DFB lasers [3-5], silicon wire waveguides [6, 7], and optical fibers [8, 9]. Amongst these nonlinear media, optical fibers are uniquely advantageous in the sense that they offer low propagation loss, long interaction lengths and are naturally compatible to the optical transmission systems. Also, the FWM wavelength conversion technique possesses a number of advantages, including (i) identical features between the converted signal and its original, (ii) continuous tuning range, (iii) modulation format independent operation and (iv) the possibility for simultaneous conversion of multiple signals. Indeed, all-fiber broadband wavelength converters based on the FWM technique are in high demand in high-speed and dense wavelength division multiplexing (DWDM) fiber-optic transmission systems.

The conversion efficiency of FWM in optical fibers strongly depends on the phase-matching between the signals, which is typically determined by the chromatic dispersion of the fiber [10]. Typically, a long length of a dispersion tailored fiber or dispersion shifted fiber (DSF) is used as the mixer for FWM and a strong wave at or near the zero dispersion wavelength (ZDW) is injected as the pump wave. In 1992, partially degenerate FWM (PDFWM) was demonstrated in a 10-km-long DSF, in which the wavelength conversion range was 7.6 nm (wavelength difference between the idler and the probe) with a conversion efficiency of -24 dB [8]. However, it was found that the FWM conversion bandwidth in optical fibers is mainly limited by (i) the dispersion variation along the fiber length, (2) the birefringence of the optical fiber and the phase-mismatch between the interactive waves [9]. Evidently, these effects could be minimized by means of using shorter optical fibers [9, 10] or tailoring of the dispersion profile of the optical fibers [11], so that the FWM wavelength

conversion range could be expanded. The former results have shown an extension of the wavelength conversion range from ~4 nm with 24.5 km long highly nonlinear DSF to ~91 nm with 100 m instead. Moreover, a 3 dB wavelength conversion bandwidth of ~100 nm has been reported in a 20 m long silica-based highly nonlinear photonic-crystal fiber (PCF) [12] and a bandwidth of ~60 nm with ~0 dB PDFWM conversion efficiency has been demonstrated in a 2.2 m long lead silicate PCF [13]. In addition to the PDFWM discussed above, non-degenerate FWM or Bragg scattering FWM with a wavelength conversion range of ~180 nm has been realized in optical fibers as well [14]. In that particular scheme, two pump waves are launched into the optical fiber simultaneously [14]. Overall, such fiber-based FWMs have the drawbacks of (i) requiring a pump source at or near the ZDW of the employed fiber, which restricts the selection of the available pump sources for FWM generation, and (ii) a narrow wavelength conversion range due to the long length of optical fiber typically needed. Hence, a more compact and more flexible method to achieve wide range wavelength conversion by using FWM in optical fibers is highly desirable.

Recently, ultra-compact FWM in a 30 cm-long R-DFB fiber laser was demonstrated [15]. Here, the generated R-DFB signal acts as the pump for the FWM and the DFB cavity significantly enhances the wavelength conversion efficiency. In this paper, we both experimentally and theoretically study the continuously tunable FWM with extended broadband wavelength conversion range in the R-DFB fiber laser [16]. Section 2 and 3 describe the experimental setup and results. Section 4 presents the simulation model. In section 5, the principle of such highly efficient FWM in the R-DFB fiber laser is theoretically analyzed.

## 2. Experimental setup

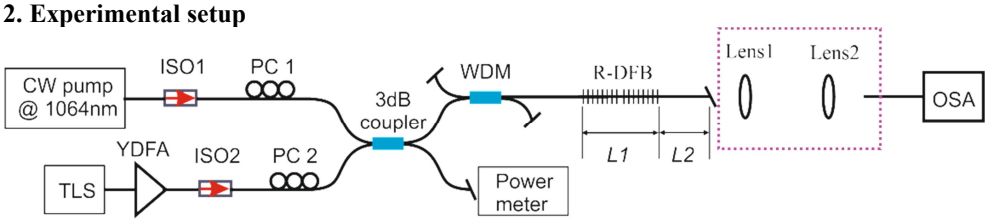


Fig. 1 Schematic diagram of experimental setup for FWM generation in a R-DFB fiber laser. ISO: isolator; PC: polarization controller; WDM: wavelength division multiplexer; TLS: tunable laser source; YDFA: Yb-doped fiber amplifier; OSA: optical spectrum analyzer.

The schematic diagram of the experimental setup is shown in Fig. 1. It consists of a high power continuous-wave (CW), linearly polarized pump source at ~1064 nm for the initial R-DFB fiber laser generation [17] and a linearly polarized TLS (DL pro, Toptica Photonics, 1040 – 1080 nm) as the probe wave for FWM generation in the R-DFB fiber laser. The TLS was amplified by a polarization maintaining (PM) Yb-doped fiber amplifier (YDFA). The output of the CW pump @1064 nm and the TLS was connected to an isolator (ISO1 and ISO2) and a polarization controller (PC1 and PC2) respectively, which was utilized to adjust their polarization states. The 1064 nm pump and the TLS signals were coupled into the R-DFB grating via a 3 dB coupler (designed for 1064 nm). A 1064/1117 nm wavelength division multiplexer (WDM) was inserted between the R-DFB grating and the 3 dB coupler in order to filter out the backward R-DFB signal. The forward output from the R-DFB grating was directly coupled into an optical spectrum analyzer (OSA) through a wavelength-independent free-space attenuator (the dotted-square box in Fig.1). All the fiber ends were angle-cleaved to prevent end-feedback and the R-DFB grating was mounted on a heat sink to help control the temperature and better remove any generated heat. Note that all the passive components as seen in Fig. 1 are non-PM and they were all mounted statically on the optical bench to reduce the influence of the environmental vibrations.

The R-DFB grating is 30 cm long with a center π phase-shift [18, 19]. It was fabricated directly into a standard single-mode fiber (SMF) (PS980 from Fibercore Ltd.) with UV light

at 244 nm using our continuous grating writing technique [20]. The coupling coefficient of the grating is 37 $m^{-1}$ [18]. A length L2 = 1.8 m of the same PS980 fiber was used as the pigtailing fiber of the R-DFB grating. The NA, propagation loss ($\alpha$) at 1.1 μm, and nonlinear coefficient ($\gamma$ @ 1.1 μm) of PS980 are 0.14, 20 dB/km and ~6 $(Wkm)^{-1}$, respectively.

### 3. Experimental results

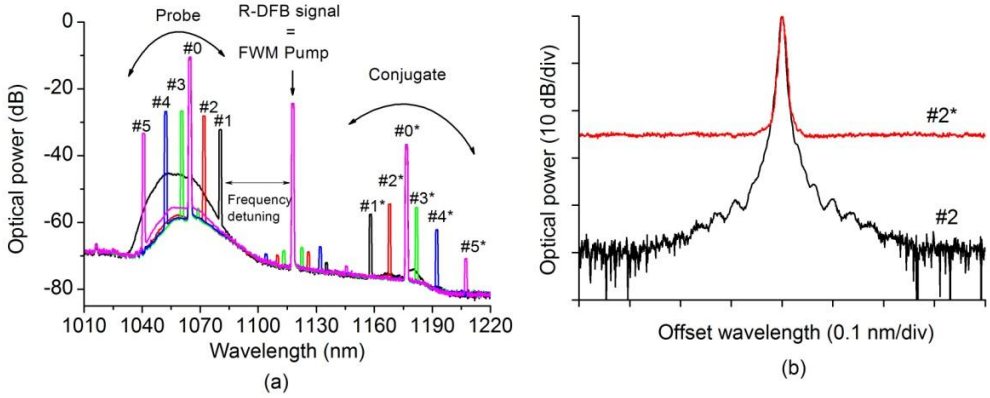


Fig. 2 (a) FWM output spectra with a resolution of 1 nm and (b) normalized overlapping spectra of the probe wave #2 and corresponding conjugate wave #2* with a resolution of 0.01 nm.

Typical FWM output spectra from the R-DFB grating with continuously tuned probe waves are shown in Fig. 2(a) measured with a resolution bandwidth (RBW) of 1 nm. As reported in previous work [19], the pump wave for the FWM process is the internal generated R-DFB signal (as indicated in Fig. 2(a)) and the conjugate wave (denoted #0*) is converted from its original wave (#0), which is the CW pump at ~1064 nm for R-DFB signal generation. When the TLS is continuously tuned from ~1080.4 nm ( #1 in Fig. 2(a)) to ~1040.8 nm ( #5 in Fig. 2(a)), the corresponding idlers at ~1158 nm (#1* in Fig. 2(a)) to ~1207.3 nm (#5* in Fig. 2(a)) appear clearly above the noise floor. The specific spectra of the probe and conjugate waves have been measured with a high RBW of 0.01 nm and are shown in Fig. 2(b). The spectral signature of the conjugate wave matches very well with its original wave within the 25 dB bandwidth, which is limited by the noise floor in the measurement. Note that the noise floor of traces #2 and #2* is only limited by the sensitivity of the employed OSA. The incident power of the probe signals is in the range of 10 to 70 mW whilst the incident power of the CW pump at ~1064 nm is maintained constantly at 2 W ± 5%. This pump power is selected due to the limitation of the maximum power provided by the CW pump source, and also, at this power level, the maximum FWM conversion efficiency has been achieved, as reported in previous work of [19].

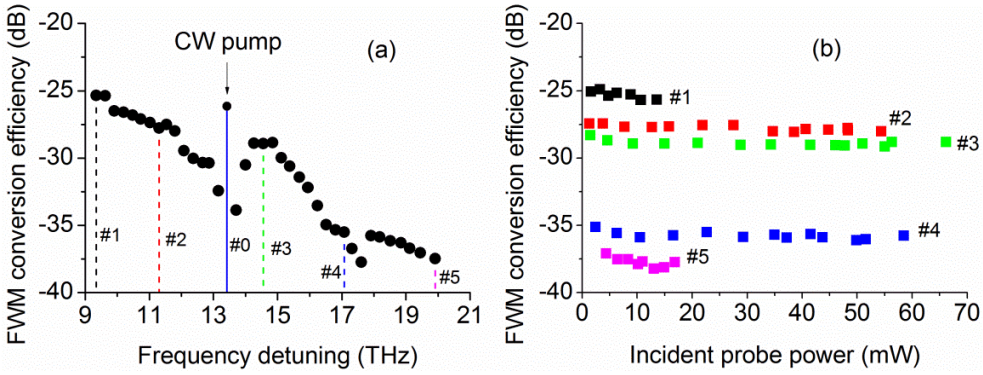


Fig. 3 (a) FWM conversion efficiency of the R-DFB fiber laser with respect to the frequency detuning. The vertical lines indicate the probe waves of #i (i = 0,1,2,3,4,5). (b) FWM conversion efficiency against incident probe power for probe waves of #1, #2, #3, #4, and #5, respectively.

Fig. 3 (a) shows the FWM conversion efficiency with respect to the frequency detuning, which is the frequency separation between the probe and FWM pump, i.e., R-DFB signal. The vertical lines indicate FWM conversion efficiency measured at the probe waves of #i (i = 0,1,2,3,4,5), as also seen in Fig. 2(a). As seen in Fig. 3 (a), the FWM conversion efficiency decreases from ~ -25 dB to ~ -37.5 dB while increasing the frequency detuning from ~9.3 THz (corresponding to the probe wave at 1080.4 nm) to ~19.9 THz (corresponding to the probe wave at 1040.8 nm). This is expected since the phase-mismatch factor increases with increasing frequency detuning [8, 21]. However, the FWM conversion efficiency remains nearly constant with varying probe power, as shown in Fig. 3(b). It can be seen clearly that the FWM conversion efficiency is constant within ± 0.7 dB fluctuations. It is therefore concluded that the reduction of the conversion efficiency in Fig. 3(a) is predominantly due to the frequency detuning, and not as a result of the power variation of the probe waves.

## 4. Analysis

In order to better understand the fundamental mechanism for the FWM process in the R-DFB fiber laser, a numerical model was built. A schematic diagram of the model is shown in Fig. 4. In the model, the design of the R-DFB grating is based on the experimental realization. As mentioned previously the R-DFB signal acts as the pump for FWM. It possesses a nonuniform intensity distribution within the DFB cavity [22-24], as seen in Fig. 4. A CW probe is launched into the R-DFB grating from the left side of the grating (i.e., z = 0), whilst the corresponding conjugate wave, as well as the remaining pump and probe are emitted from the right side of the R-DFB grating (i.e., z = *L*).

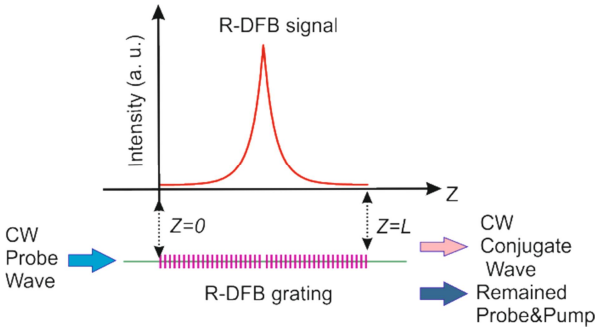


Fig. 4 Schematic diagram of theoretical model setup for FWM in R-DFB fiber laser.

For simplicity, several approximations are adopted for the simulation. Firstly, the pump (i.e. R-DFB signal) is assumed to be undepleted during the FWM process within the R-DFB grating, since the experimental FWM conversion efficiency is less than 1%. Secondly, the forward R-DFB signal is assumed to be identical to the backward R-DFB signal, since the phase-shift of the DFB is placed at the center of the grating. Hence, the amplitudes of the forward, $A_{1f}(z)$, and backward, $A_{1b}(z)$, R-DFB signals along the DFB grating length of $L$ are given by Eqs. (1) and (2) [23], where κ is the coupling coefficient of the DFB grating. Thirdly, single-mode fiber is utilized and all the overlap integrals of the waves are assumed to be identical to $1/A_{eff}$, where $A_{eff}$ is the effective mode area of fiber [21]. Therefore, the coupled amplitude equations for the FWM process in the R-DFB fiber laser are obtained, as described by Eqs. (3) and (4), in which $A_3, A_4$ are the amplitudes of probe and conjugate waves, respectively, and $A_j \equiv \sqrt{P_j / A_{eff}}$, $(j = 1f, 1b, 3, 4)$.

$$A_{1f}(z) = \begin{cases} A_{1f}(z=L)\cdot\sinh(\kappa z) & z < L/2 \\ A_{1f}(z=L)\cdot\cosh[\kappa(L-z)] & z > L/2 \\ A_{1f}(z=L)\cdot[\sinh(\kappa L/2)+\cosh(\kappa L/2)]/2 & z = L/2 \end{cases} \quad (1)$$

$$A_{1b}(z) = \begin{cases} A_{1b}(z=0)\cdot\cosh(\kappa z) & z < L/2 \\ A_{1b}(z=0)\cdot\sinh[\kappa(L-z)] & z > L/2 \\ A_{1b}(z=0)\cdot[\sinh(\kappa L/2)+\cosh(\kappa L/2)]/2 & z = L/2 \end{cases} \quad (2)$$

$$dA_3/dz = i\gamma_3[(|A_3|^2 + 2|A_{1f}|^2 + 2|A_{1b}|^2 + 2|A_4|^2)\cdot A_3 + {A_{1f}}^2 A_4^* e^{-i(\delta k)z}] - \alpha_3 A_3/2 \quad (3)$$

$$dA_4/dz = i\gamma_4[(|A_4|^2 + 2|A_{1f}|^2 + 2|A_{1b}|^2 + 2|A_3|^2)\cdot A_4 + {A_{1f}}^2 A_3^* e^{-i(\delta k)z}] - \alpha_4 A_4/2 \quad (4)$$

The first four terms on the right side of Eqs. (3-4) describe the Kerr effect of self-phase modulation (SPM) and cross-phase modulation (XPM), in which $\gamma_i = 2\pi n_2/\lambda_i, (i = 3,4)$ is the nonlinear coefficient at the wavelength of probe ($\lambda_3$) and conjugate wave ($\lambda_4$). The last terms in Eqs. (3-4) represent the linear background losses of the probe wave ($\alpha_3$) and conjugate wave ($\alpha_4$) in the R-DFB cavity. The remaining terms in Eqs. (3-4) represent the parametric FWM interaction, in which $\delta k$ is the phase mismatch parameter. The boundary conditions for the simulations are given in Eq. (5), in which $P_{1f}(z=L)$ is the output power of the R-DFB signal and $P_3(z=0)$ is the incident power of the probe wave.

$$\begin{gathered} A_{1f}(z=L) = A_{1b}(z=0) = \sqrt{P_{1f}(z=L/A_{eff})} \\ A_3(z=0) = \sqrt{P_3(z=0/A_{eff})} \\ A_4(z=0) = 0 \end{gathered} \quad (5)$$

The coupled amplitude equations (3-4) are numerically solved using a fourth-order explicit Runge-Kutta method with MATLAB. In the simulation, we use system parameters based on the experiment, as summarized in Table 1. Note that the background losses of the involved waves are assumed to be identical as 20 dB/km. Therefore, the FWM conversion efficiency can be calculated as:

$$\eta = P_4(z=L)/P_3(z=L) \quad (6)$$

Table 1 Main parameters applied for FWM simulation in the R-DFB fiber laser

| Parameter | $P_{1f}(z=L)$ (mW) | $P_3(z=0)$ (mW) | $\kappa$ ($m^{-1}$) | $A_{eff}$ ($\mu m^2$) | $n_2$ ($m^2/W$) | $L$ (cm) | $\alpha$ (dB/km) |
|---|---|---|---|---|---|---|---|
| Value | 60 | 50 | 37 | 35 | $3.2\times10^{-20}$ | 30 | 20 |

## 5. Simulation results

Fig. 5(a) shows the evolution of the calculated FWM conversion efficiency with respect to the phase mismatch factor, $\delta k$, from the 30 cm long R-DFB fiber laser and the same length (30 cm) of bare fiber, respectively. It can be found that the maximum FWM conversion efficiency is -17.6 dB from the R-DFB fiber laser, whilst it is only -80 dB from the bare fiber. Obviously, the FWM parametric effect has been significantly enhanced in the R-DFB fiber cavity. This is mainly because (i) the intensity of the pump (R-DFB signal) has been greatly enhanced, as shown in Eqs. (1-2); and (ii) the dispersion at the pump wavelength (R-DFB signal) has been modified by the DFB grating structure [25]. The ZDW of PS980 is at around 1.48 μm, indicating that the operation wavelengths are within the normal dispersion regime of the fiber, as seen in Fig. 5(b). However, the grating dispersion reaches very high values within the narrow pass-band (in the order of kHz) of the DFB grating around the R-DFB wavelength whilst the grating dispersion is negligible for the waves far outside the pass-band, as shown in Fig. 5(b). Hence, in this scenario, the phase mismatch factor, $\delta k$, is the outcome of the combination of the fiber dispersion ($\delta k_F$) and the DFB grating dispersion ($\delta k_{FBG}$), i.e., $\delta k = \delta k_F + \delta k_{FBG}$. For example, when the frequency detuning is 13.4 THz, the fiber dispersion $\delta k_F$ is calculated to be ~146 $m^{-1}$ and the FWM conversion efficiency is demonstrated as -25.6 dB, as seen in Fig. 3(a). For this conversion efficiency, the $\delta k$ can be deduced to be 65 $m^{-1}$ from Fig. 5(a), indicating by the dashed lines. So, the DFB grating contributes a negative phase mismatch factor, i.e., $\delta k_{FBG}$ = -81 $m^{-1}$, on the FWM generation in the R-DFB cavity.

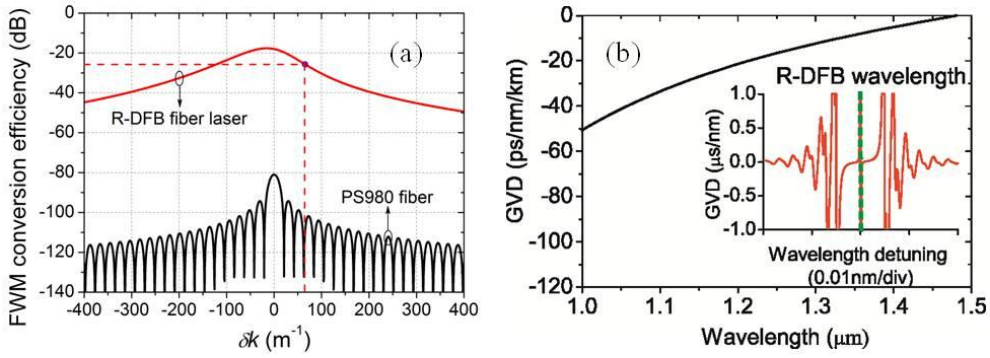


Fig. 5 (a) Calculated FWM conversion efficiency in the 30 cm long R-DFB fiber laser and a similar length of PS980 fiber, respectively; (b) Calculated dispersion profile of the PS980 fiber (inset shows the calculated dispersion of the R-DFB grating).

Considering the dispersions of the fiber and DFB grating together, the FWM conversion efficiency with respect to the frequency detuning with varied grating dispersion factor, $\delta k_{FBG}$, is plotted in Fig. 6(a). For comparison, the experimental data of the FWM conversion efficiency are plotted in Fig. 6(a) as well. Overall, the experimental data follow a similar trend to that of the simulated data and match well with the simulation results given $\delta k_{FBG}$ varying within the range of 0 to -120 $m^{-1}$. Furthermore, Fig. 6(b) shows the FWM conversion efficiency against the probe power from several mW to 5 W given the $\delta k$ = 65 $m^{-1}$. It is

evident that the FWM conversion efficiency remains constant, which is in good agreement with the experimental data illustrated in Fig. 3 (b).

Fig. 7 (a) illustrates the FWM conversion efficiency as a function of the coupling coefficient of the DFB grating with a length of 30 cm. The κ value of the experimental demonstration is indicated by the vertical dashed line. It can be seen that the FWM conversion efficiency grows and peaks as the κ increases up to ~39 $m^{-1}$. This we believe is due to the shorter effective cavity length of the DFB cavity for a stronger κ [17]. On the other hand, for a constant κ, the FWM conversion efficiency is bigger for a smaller phase mismatch factor, $\delta k$, which can also be seen in Fig. 5(a). In addition, the evolution of the FWM conversion efficiency with respect to the length of the DFB grating with a constant κL = 11.1 has been calculated, as shown in Fig. 7(b). Evidently, the peak conversion efficiency can be increased from -30 dB to -10 dB by increasing the length from 10 cm to 90 cm. However, it should be noted that the wavelength conversion bandwidth is inversely proportional to the length of the DFB grating.

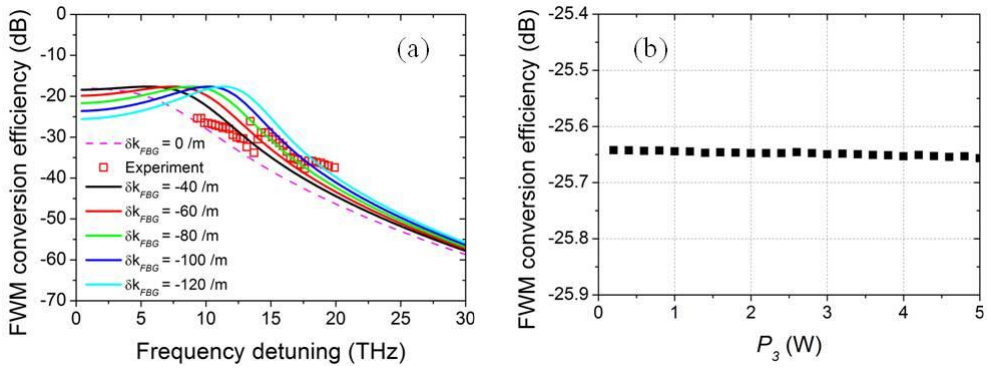


Fig. 6 (a) Comparison of the experimental and calculated FWM conversion efficiency against frequency detuning; (b) Calculated FWM conversion efficiency against probe power from several mW to 5 W.

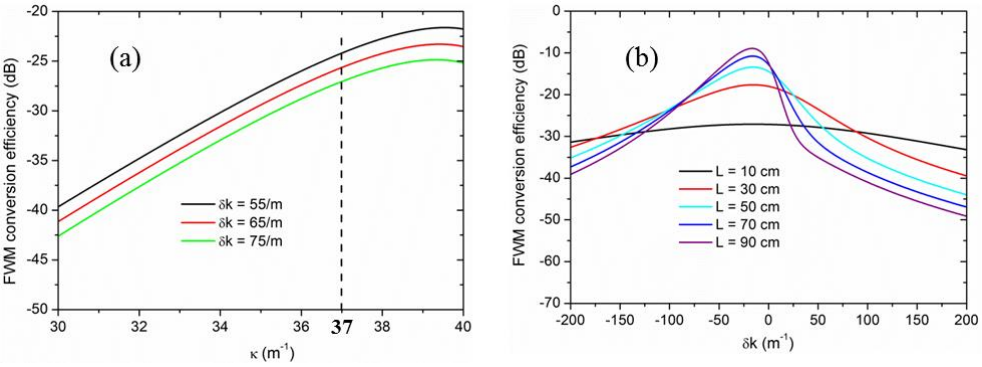


Fig. 7 Calculated FWM conversion efficiency against (a) coupling coefficient of the DFB grating and (b) length of the DFB grating.

## 6. Conclusions

We have demonstrated up to 40 THz wavelength conversion in a 30 cm long R-DFB fiber laser formed in a commercially available Ge/Si optical fiber, PS980. Such a broadband and highly efficient wavelength conversion is attributed to the significantly enhanced field-distribution of the R-DFB signal in the DFB grating cavity and the dispersion introduced by the DFB structure. This has been confirmed by simulations. The simulation results also indicate that the FWM conversion efficiency could be further increased by reducing the phase mismatch factor, and/or increasing the coupling coefficient and/or the length of the DFB grating. By using a shorter DFB grating, e.g. 10 cm, the wavelength conversion bandwidth could be enlarged at the cost of the conversion efficiency. Above all, the R-DFB fiber laser is a promising candidate for a compact, flexible and ultra-wide bandwidth wavelength converter.